Uranium extraction using magnetic nano-based particles of diethylenetriamine-functionalized chitosan: Equilibrium and kinetic studies

Mohammad G. Mahfouz, Ahmed A. Galhoum, Nabawia A. Gomaa, Sayed S. Abdel-Rehem, Asem A. Atia, Thierry Vincent, Eric Guibal

Uranium extraction using magnetic nano-based particles of diethylenetriamine-functionalized chitosan: Equilibrium and kinetic studies

Mohammad G. Mahfouz [a], Ahmed A. Galhoum [a,b,*], Nabawia A. Gomaa [a], Sayed S. Abdel-Rehem [c], Asem A. Atia [d], Thierry Vincent [b], Eric Guibal [b,*]

[a] *Nuclear Materials Authority, P.O. Box 530, El-Maadi, Cairo, Egypt*
[b] *Ecole des Mines Alès, Centre des Matériaux des Mines d'Alès, 6 avenue de Clavières, Alès cedex, France*
[c] *Chemistry Department, Faculty of Science, Ain Shams University, Egypt*
[d] *Chemistry Department, Faculty of Science, Menoufia University, Egypt*

HIGHLIGHTS

- Magnetic chitosan nanoparticles grafted with diethyleneamine were synthesized.
- U(VI) sorption from sulfuric acid solutions is exothermic and spontaneous.
- Langmuir equation fits sorption isotherms.
- Uptake kinetics is modeled by the pseudo-second order rate equation.
- U(VI) is efficiently desorbed with acidic urea solutions; sorbent can be recycled.

GRAPHICAL ABSTRACT

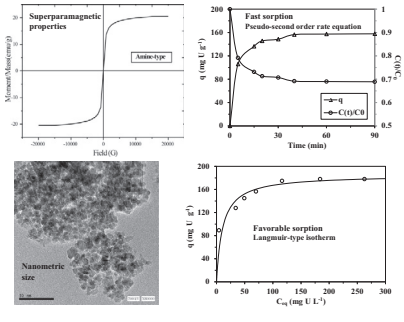

Keywords:
Adsorption
Uranium(VI)
Magnetic amine-functionalized chitosan nano-based particles
Kinetics
Isotherms

ABSTRACT

Magnetic nano-based particles of diethylenetriamine-functionalized chitosan have been synthesized before being characterized by elemental analysis, FT-IR spectroscopy, XRD, AFM, TEM and VSM analysis. Uranium adsorption (from synthetic solutions) has been investigated in batch systems. The effects of dif-ferent experimental parameters such as initial solution pH (controlled with sulfuric acid), equilibration time, initial uranium concentration and temperature on sorption performance have been determined. The nano-based particles, with size in the range 10–30 nm, are super-paramagnetic. The kinetic data can be efficiently modelled using the pseudo-second-order equation. The Langmuir and the Dubinin–Radushkevich (D–R) equations fit well sorption isotherms. The value of activation energy (E_{DR} = 8.39 kJ/mol) indicates that the process is associated to chemical interactions (rather than pure physical sorption). In addition the values of thermodynamic parameters ($\Delta G°$ and $\Delta H°$) show that the process is spontaneous and exothermic. The positive value of $\Delta S°$ means that the randomness of the sys-tem increased with sorption. Finally, the adsorbent can be efficiently regenerated and recycled for at least 5 cycles using acidified urea as the eluent.

* Corresponding authors at: Ecole des mines d'Alès, Centre des Matériaux des mines d'Alès, 6 avenue de Clavières, F-30319 Alès cedex, France (E. Guibal), National Materials Authority, P.O. Box 530, El-Maadi, Cairo, Egypt (A.A. Galhoum).
E-mail addresses: Galhoum_nma@yahoo.com (A.A. Galhoum), Eric.Guibal@mines-ales.fr (E. Guibal).

1. Introduction

The mining of uranium ores and their hydrometallurgical processing produce aqueous waste streams containing different metal ions, with concentrations levels that frequently exceed authorized discharge levels. Bioleaching and chemical leaching, producing sulfuric acid, contribute to solubilize uranium from infra-marginal waste ores, prior to their discharge into tailing ponds, leading to possible metal release into the environment [1–4]. On the other hand, the resources (uranium mines) are rather limited and the expected shortage of uranium in the near future contribute to make the mining, production, and separation of this metal a strategic issue [5]. The recovery of uranium from dilute aqueous streams represent an important challenge for these environmental and economic reasons. While conventional processes such as precipitation or solvent extraction processes face economical or technical limitations for the treatment of dilute metal solutions, mineral sorbents [6,7], ion-exchange and chelating resins [5,8–10] may be more appropriate. Biosorption has recently attracted a lot of attention as an alternative to conventional synthetic resins for the recovery of metal ions from low-concentration effluents [11–13]. Though the objective in biosorption process is using very cheap materials for metal recovery, sometimes their poor properties in terms of sorption capacities, and/or poor applicability at large scale (head loss pressure and clogging in fixed-bed systems) are incentive to using more elaborated products issued from these biomass (such as biopolymers extracted from crustacean shells or from algal biomass) [14–16].

Chitosan is the deacetylated form of chitin (a linear polymer of N-acetyl-D-glucosamine). It is hydrophilic, biodegradable and harmless; in addition, this biopolymer bears many amino and hydroxyl groups that can bind heavy metal ions through different mechanisms, including ion-exchange and electrostatic attraction for metal anions in acidic solutions or chelation of metal cations in near-neutral solutions [16]. The presence of these hydroxyl and amine groups is also very important for the easy chemical modification of the biopolymer [17]. Therefore, chitosan reveals a very promising starting material for manufacturing chelating resins [18]. The grafting of new functional groups on the backbone of chitosan may increase the density of sorption sites, change the mechanism of sorption, the range of pH for efficient sorption and the selectivity for target metals [19,20]. Complex amine groups (such as tetraethylenepentamine or diethylenepentamine) have been frequently grafted on chitosan to improve the sorption properties of the biopolymer backbone [21–26].

One of the most limiting properties of chitosan for metal sorption is the poor porosity of the sorbent that requires decreasing the size of the particles (with difficulty for removing particles from treated effluents, or in operating the system in fixed-bed columns) or changing the conditioning of the biopolymer (preparing for example gel beads or foams) to improve mass transfer properties [16,27]. Recently, nanomaterials have received a great attention for the synthesis of new sorbents: nano-sized adsorbents possess quite good performance due to their high specific surface area and the absence of resistance to intraparticle diffusion [18]. The main problem at using nano-based particles consists in sorbent dispersion and difficulty in recovering the spent material; this problem can be overcome by associating a magnetic core (embedded in the reactive polymeric shell) to these nanoparticles: the spent material can thus be recovered at the end of the process by an external magnetic field [28–30].

In the present study, magnetic chitosan nano-based particles have been functionalized with diethylenetriamine (DETA, bearing chelating amine moieties) using epichlorohydrin as the cross-linking agent. This sorbent was characterized by elemental analysis, FT-IR spectrometry, X-ray diffraction (XRD), atomic force microscopy (AFM), transmission electron microscopy (TEM) and vibrating sample magnetometry (VSM). In a second step the sorption properties for uranium (from aqueous solutions with pH controlled by sulfuric acid) were characterized in batch systems for the evaluation of sorption isotherms, uptake kinetics and thermodynamic properties. The regeneration and recycling of the sorbent was finally tested. These parameters are critical for the scaling-up of the process before investigating sorption properties in continuous systems.

2. Experimental

2.1. Reagents and analysis

Chitosan (90.5% deacetylation degree) was purchased from Sigma–Aldrich (France). Diethylenetriamine (98%) was obtained from Sigma–Aldrich, epichlorohydrin (>98%), 1,4-dioxane (99.9%) and ethanol were supplied by Fluka Chemicals. Arsenazo III (analytical grade reagent) was obtained from Fluka Chemicals while all other chemicals were Prolabo products (used as received). Uranium stock solution was prepared from $UO_2(OCOCH_3)_2{\cdot}2H_2O$, supplied by Sigma–Aldrich, dissolved in concentrated sulfuric acid under heating and finally diluted in demineralized water (concentration: 1000 mg U L^{-1}). The solutions were prepared by appropriate dilution of the stock solutions immediately prior to use. Uranium concentrations in both initial and withdrawn samples were determined by spectrophotometry using Arsenazo III colorimetric method [31] and a UV–Visible spectrophotometer (Metertech Inc, model SP-8001). The pH of the uranium solutions was adjusted using either 0.2 M NaOH or 0.2 M H_2SO_4 solutions when low pH changes were required, and 0.5 M solutions of acid/base titrating agent when larger pH variations were targeted.

2.2. Synthesis of the sorbent

2.2.1. Manufacturing of magnetic cross-linked chitosan nano-based particles

Magnetic chitosan nanoparticles were prepared by chemical co-precipitation of Fe(II) and Fe(III) ions by NaOH, in the presence of chitosan, followed by hydrothermal treatment [32]. Chitosan (4 g) was dissolved in 200 mL (20% w/w) acetic acid solution before adding $FeSO_4$ and $FeCl_3$ salts (1:2 molar ratio Fe(II)/Fe(III)) and the resulting solution was chemically precipitated at 40 °C by adding 2 M NaOH dropwise under constant stirring; the pH being controlled to 10–10.4. The suspension was heated at 90 °C for 1 h under continuous stirring before being separated by decantation (and magnetic attraction). In the next step, an alkaline solution of 0.01 M epichlorohydrin (in 0.067 M NaOH) was prepared (pH ≈ 10) and added to a freshly-prepared suspension of wet magnetic-chitosan nano-based particles (the mass ratio was 1:1). The mixture was heated for 2 h under constant stirring at 40–50 °C [33]. The material (ii) was finally filtered and extensively washed with demineralized water to remove any unreacted epichlorohydrin.

The diethylenetriamine moiety was grafted on cross-linked magnetic nano-based particles of chitosan in two steps. First, the cross-linked chitosan (ii) was suspended in 150 mL of ethanol/water mixture (1:1 v/v) and epichlorohydrin (15 mL) was added to the suspension under agitation and reflux for 4 h [34]. The product (iii) was then filtered and washed three times successively with ethanol and ultrapure water to remove any residual reagent. In the next step, the product (iii) was suspended in 200 mL ethanol/water mixture (1:1 v/v) and 12 mL of diethylenetriamine were added.

The mixture was stirred at 75–80 °C for 18 h [35]. After the reaction, the final product was filtered off and extensively washed three times successively with ethanol and ultrapure water. Finally, the sorbent was freeze-dried for about 24 h.

The amine content in the sorbent was estimated using a volumetric method [35]: 30 mL of 0.05 M HCl solution was added to 0.1 g of the sorbent and maintained under agitation for 15 h on a shaker. The residual concentration of HCl was estimated by titration against 0.05 M NaOH solution and phenolphthalein as the indicator. The number of moles of HCl having reacted with amino group (and consequently the amino group concentration, mmol/g) was calculated from Eq. (1):

$$\text{Concentration of amino group} = (M_1 - M_2) \times 30/0.1 \quad (1)$$

where M_1 and M_2 are the initial and final concentrations of HCl, respectively.

2.2.2. Characterization methods

The chemical composition of the resin (i.e., C, H and N contents) was characterized using an automatic analyzer (CHNS Vario EL III-elementar analyzer, Elementar, Germany). Powder X-ray diffraction (XRD) patterns were obtained at room temperature using a Philips X-ray generator model PW 3710/31 (Philips, Japan) with the Cu K_α radiation, in the range 2θ = 10–90°. The magnetic properties were determined on a vibrating sample magnetometer (VSM) (730T, Lakeshoper, America) at room temperature. The dimension and morphology of the sorbent were analyzed by atomic force microscopy (AFM) (WET-SPM, Shimadzu, Japan) and high resolution transmission electron microscope, HRTEM, JEOL-2100 (Japan). The functional groups of the sorbent were analyzed with a Fourier Transform infrared spectrometer (Nexus 870 FTIR spectrometer, Nicolet, USA). The samples were incorporated in KBr pellets and the scanning range was set between 4000 and 400 cm^{-1}.

2.3. Sorption and desorption experiments

Batch experiments were carried out by contact of 0.02 g of functionalized-chitosan sorbent with 100 mL of aqueous solution (metal concentration, C_0: 110 mg U L^{-1}) in a stopper conical flask. The samples were agitated (at 200 rpm) for 2 h at 25 ± 1 °C. After equilibration and phase separation, the residual uranium concentration (C_{eq}, mg U L^{-1}) in the aqueous phase was determined, whilst the concentration of metal ions sorbed onto the functionalized chitosan (sorption capacity, q_e, mg U g^{-1}) was obtained by the mass balance equation (Eq. (2)):

$$q_e = (C_0 - C_{eq}) \times V/M \quad (2)$$

The distribution coefficient K_d is another specific parameter that gives an evaluation of the separation efficiency of the sorbent for the target metal:

$$k_d = q_e/C_{eq} = [(C_0 - C_{eq})/C_{eq}] \times V/M \quad (3)$$

where V is the volume of the solution (0.1 L) and M is the mass of the sorbent (0.02 g). All the measurements were duplicated. More generally, most of these experiments were duplicated or triplicated and the experimental variation was systematically less than 7%.

The optimization of the process requires investigating a series of steps such as: (a) study of pH effect, (b) uptake kinetics, (c) sorption isotherms (including the effect of temperature on process thermodynamics), and (d) regeneration/recycling of the resins. This information is fundamental for understanding the mechanisms of sorption but also the technical and economic limitations of the process (pH range of application, life cycle of the sorbent, etc.).

Standard experimental conditions were set at T: 25 ± 1 °C and pH: 3.61 ± 0.01; the contact time was fixed to 40 min. Indeed, preliminary studies have shown that an extended contact time (up to 180 min) does not significantly change sorption performance (Fig. AM1, see Additional Material Section). However, when relevant, these parameters were varied for determining pH effect, sorption isotherm characteristics and uptake kinetics. In addition, the recycling of the sorbents was tested by comparing the sorption capacity at different successive steps in a series of 5 sorption/desorption cycles: 0.02 g of sorbent was mixed with 100 mL of a uranyl solution (C_0: 200 mg U L^{-1}) for 40 min at 25 °C in a conical flask. After magnetic separation the sorbent was recovered and the uranium concentration in the supernatant was determined by the mass balance equation. The metal-loaded sorbent (after being washed with demineralized water) was mixed with 50 mL of a 0.5 M urea (acidified) solution for 30 min at 25 °C. The metal concentration in the supernatant was used for calculating the desorption yield at each step (by the mass balance equation). The concentration of sulfate anions in the investigated pH range was determined (i.e., in the range 3.6–5.0 mmol L^{-1}) using the barium precipitation method (turbidimetry analysis) [31].

3. Results and discussion

3.1. Preparation of magnetic chitosan nanoparticles

Magnetic chitosan nano-based particles were synthesized by a one-step and *in situ* co-precipitation method: Fe(II) and Fe(III) ions were initially mixed in an acidic chitosan solution before being simultaneously precipitated with chitosan using NaOH for pH control. This simple procedure produced magnetic chitosan particles of nanometric size [32]. Chitosan being soluble in acidic solutions (with the remarkable exception of sulfuric acid solutions) it can be pertinent cross-linking the material to prevent its dissolving. In addition, the chemical modification of chitosan may be used to increase the sorption capacity or change the field of application of the biosorbents (in terms of pH, metal selectivity etc.) [16]. Frequently, glutaraldehyde is used for these chemical modifications at the expense of a decrease in the availability of amine groups [36]: the reaction of aldehyde groups (on both sides of the cross-linking agent) with amine groups limits their reactivity for metal complexation [37], though this parameter has less effect on metal binding when ion exchange/electrostatic attraction mechanism is involved in metal binding [38]. In order to reduce the possible limitation in the reactivity of amine groups, epichlorohydrin was used as the cross-linking agent. Indeed, for this mono-functional cross-linker the reaction takes place with a carbon neighboring one of the hydroxyl groups of chitosan: the epoxide ring is opened and a chlorine atom is leaving to make possible the interaction with other functional groups [39]. Diethylenetriamine (DETA) had been investigated for the modification of different supports (including silica gel [40], polyacrylonitrile [41], and chitosan [42]) in order to increase their metal sorption properties. In the case of chitosan modification with DETA, Khan et al. [42] used glycidylmethacrylate as the cross-linker. Fig. 1 shows the proposed route for the synthesis of DTA-functionalized chitosan using epichlorohydrin.

To prevent the aggregation of nano-based objects during the synthesis a strong agitation (about 950 rpm) was used in order to minimize magnetic dipole–dipole effect.

3.2. Characterization of magnetic chitosan nanoparticles

The comparison of elemental analyses for both magnetic chitosan particles and magnetic functionalized-chitosan particles clearly shows the efficient chemical modification of the

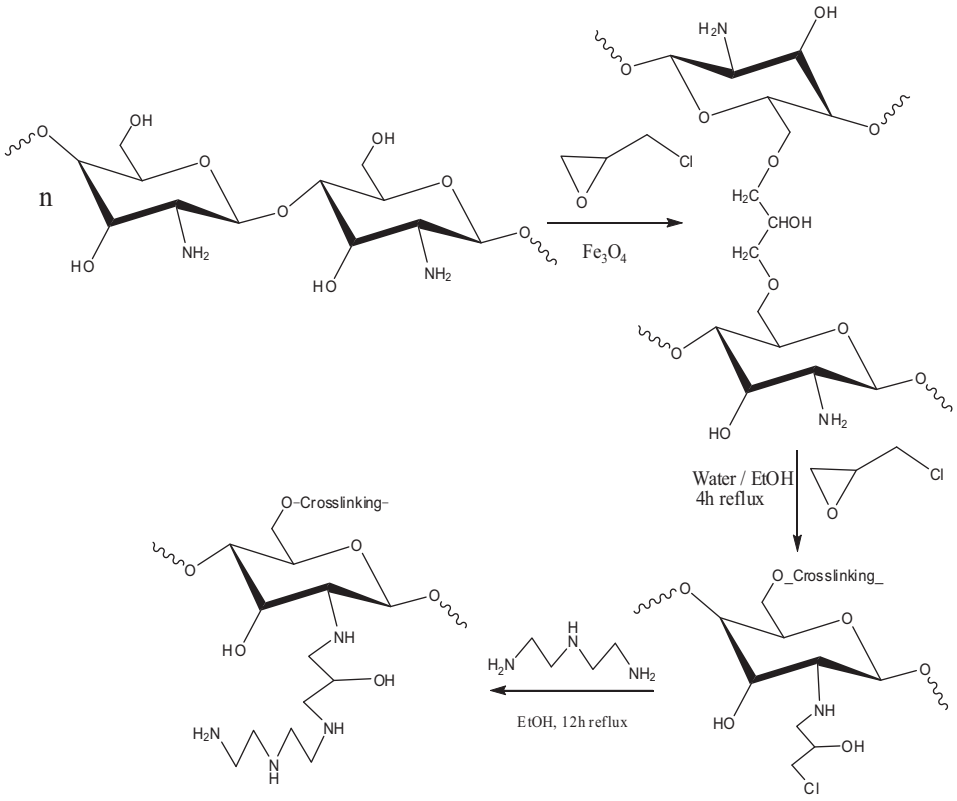

Fig. 1. Scheme for the synthesis of DETA-functionalized magnetic chitosan nano-based particles.

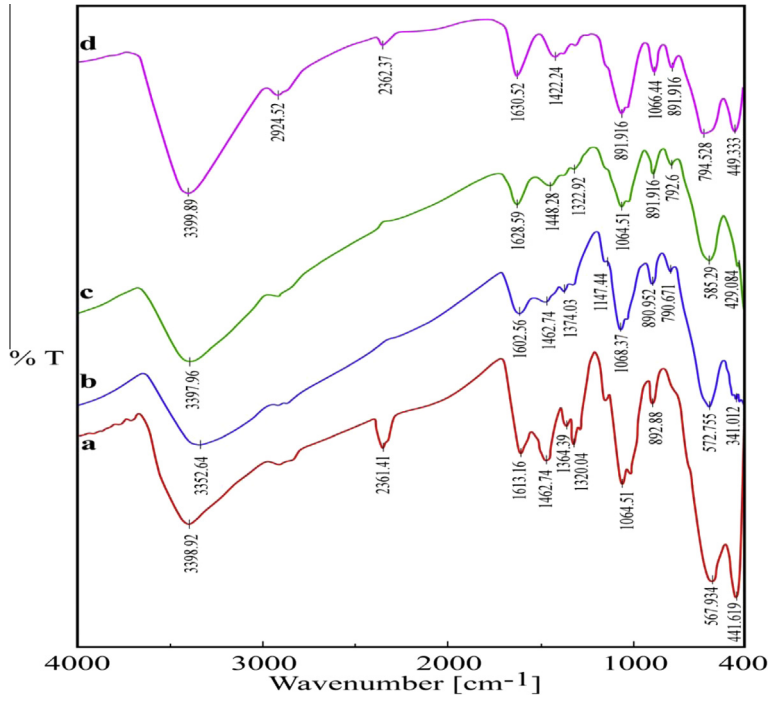

Fig. 2. FT-IR spectra of (a) magnetic chitosan nanoparticles, (b) cross-linked magnetic chitosan nano-based particles, (c) cross-linked magnetic chitosan nanoparticles with spacer arm and (d) DETA-functionalized magnetic chitosan nanoparticles.

biopolymer. Indeed, C, H and N contents varied from 14.23%, 2.55% and 1.71%, respectively, to 18.09%, 2.76% and 4.77%, respectively (after DETA grafting via the armed spacer; i.e., epichlorohydrin).

Infra-red spectroscopy was used for characterizing the functional groups on the sorbent at the different steps of the synthesis procedure (Fig. 2). Basically, the different spectra were very

similar; the main differences were identified in terms of relative intensity. The presence of iron magnetite can be correlated to the appearance of the band at 568 cm^{-1}, which is assigned to the Fe–O stretching vibration of Fe_3O_4 [32,43]. A large band appears on the spectrum of magnetic chitosan around 3399 cm^{-1}: this band is associated to the combination of contributions from stretching vibration of –OH groups, extension vibration of N–H groups, and inter hydrogen bonds of polysaccharides. Amine groups are appearing at 1613 cm^{-1}, while the stretching vibrations of primary –OH and secondary –OH groups are identified at 1320 and 1065 cm^{-1}, respectively. The bands at 1463 and 1364 cm^{-1} can be assigned to C–O–C stretching and –OH bending vibrations, respectively. The β-D-glucose unit is identified by the band at 893 cm^{-1} [20]. The cross-linking of chitosan with epichlorohydrin is confirmed by (a) the decrease in the intensity of $–NH_2$ and –OH groups (compared to reference magnetic chitosan material) [43], and (b) the appearance of a new band at 523 cm^{-1}, assigned to the stretching vibration of $–CH_2–Cl$. The intensity of the band at 792 cm^{-1} (associated to the $–CH_2–Cl$ group in cross-linked magnetic chitosan material) decreased after grafting diethyleneamine at the end of the spacer arm. On the other hand, this grafting induced an increase in the intensity of the band at 1387 cm^{-1} [44]. The variation in the intensity of the bands relative to amine groups can be correlated to the results of elemental analysis: the functionalized material contains about 4.54 mmol $–NH\ g^{-1}$: this is about 1.59 times greater than the amount found on reference magnetic chitosan particles.

Fig. 3 reports the XRD patterns of the DETA-functionalized magnetic chitosan nano-based particles: the eight characteristic peaks of Fe_3O_4 are identified by their indices: (111), (220), (311), (400), (422), (511), (440), and (622). These peaks are consistent with the database in JCPDS file (PDF No. 65-3107) [43]: this corresponds to the existence of iron oxide particles (Fe_3O_4) with a spinel structure. This confirms the magnetic properties of the sorbent and its capacity to be separated by magnetic separation. XRD patterns were also used for determining the size of the nanoparticles: the half width at half maximum is correlated to the particles size using the Debye–Scherrer equation [45]:

$$D = k\lambda/\beta\cos\theta \quad (4)$$

where D is the average diameter of nanoparticles (nm), λ is the wavelength of X-ray radiation (1.5418 Å), θ is the angle of diffraction, k = 0.9 (a shape factor) and β is the full width at half maximum of X-ray diffraction peaks. The crystal size was found to be about 6.5 nm for the sorbent (using the peak corresponding to the (311) index).

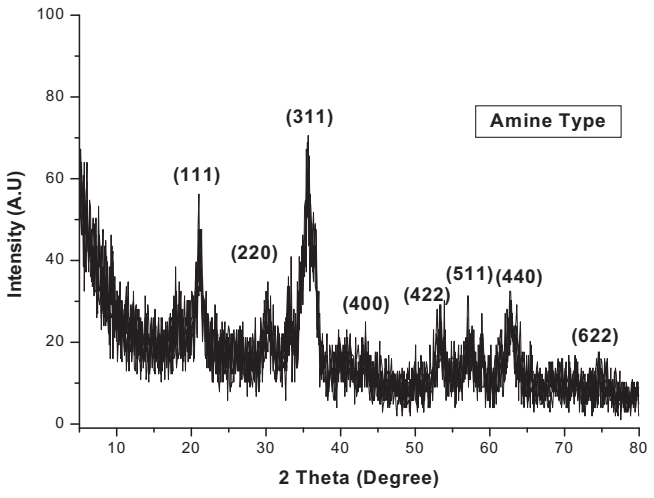

Fig. 3. Powder X-ray diffraction (XRD) pattern of DETA-functionalized magnetic chitosan nano-based particles.

Atomic force microscopy (AFM) is a useful tool for analyzing the topography of adsorbent at nanoscale. Fig. 4a and b shows the 2-D and 3-D images of the surface of the sorbent. The scanning area is 5 × 5 μm and the surface of quartz substrate was completely covered by the nanoparticles. The surface is homogeneous and small light dots are identified: the size of the irregular points remains quite small in height (a few nm). The physical aggregation of magnetic nano-based particles observed at the surface of the quartz substrate can be probably attributed to the magnetic forces existing between the particles and this is reinforced by the small size of the particles with high surface energy [46].

The TEM image of the sorbent is shown in Fig. 4c: the particles have a spherical morphology and are homogeneous (both in size and shape). The structure of the adsorbent was monodisperse, but the particles tend to form agglomerate of 10–30 nm width. This agglomeration may be explained by the strong aggregation of the particles due to the strong magnetic dipole-dipole attraction between particles. TEM images also show contrasted areas for chitosan–Fe_3O_4 particles: the dark areas represent crystalline Fe_3O_4 while the bright ones are associated with chitosan (and chemically modified chitosan). This can be explained by the difference in the electron-absorbing ability of magnetic iron core and chitosan-shell compartments [47]. The size of nano-based magnetic particles is hardly affected by chitosan coating based on the difference of size for biopolymer-coated particles and non-coated particles. The homogeneous distribution of the coating agent and the homogeneous shape of the nano-objects tend to indicate that the grafting of the spacer end of the DETA on chitosan does not contribute to significantly aggregate the particles: this can be explained by the strong agitation selected during the synthesis of the material.

The magnetic properties of synthesized sorbent were determined using VSM (vibrating sample magnetometry), Fig. 5 shows the typical magnetization loop: the sample does not exhibit remanence and coercivity. This means that magnetic chitosan nanoparticles are super-paramagnetic. The saturation magnetization was calculated to be close to 20.5 emu/g. Therefore, the magnetic chitosan nanoparticles will be easily separated with the help of an external magnetic field.

3.3. Uranium adsorption properties

The properties of the synthesized sorbent were tested for uranyl (UO_2^{2+}) sorption beginning with the effect of pH and uptake kinetics; sorption isotherms were determined at different temperatures for evaluating thermodynamic characteristics. Metal desorption and resin recycling were finally tested.

3.3.1. Effect of pH and interpretation of sorption mechanisms

The pH of the aqueous solution plays an important role in the whole sorption process and particularly on sorption capacity. Indeed; it may influence the surface charge of the sorbent, the degree of ionization of the material, and the dissociation of functional groups such as carboxyl, hydroxyl and amino groups present at the surface of the sorbent [48]. It can also influence the aqueous chemistry of uranium [11]. The influence of initial solution pH was investigated within the range 1.56 ± 0.01 to 6.66 ± 0.01, adjusted by using either 0.5 M H_2SO_4 or 0.5 M NaOH (or 0.2 M H_2SO_4 or 0.2 M NaOH) solutions. At pH higher than 6.66, precipitation of uranyl ions (under the form $UO_2(OH)_2$) would occur spontaneously, and below pH 1.65, the inorganic magnetic matter tends to dissolve.

Fig. 6 shows the impact of initial pH on both sorption capacity and equilibrium pH. This figure clearly confirms the strong impact

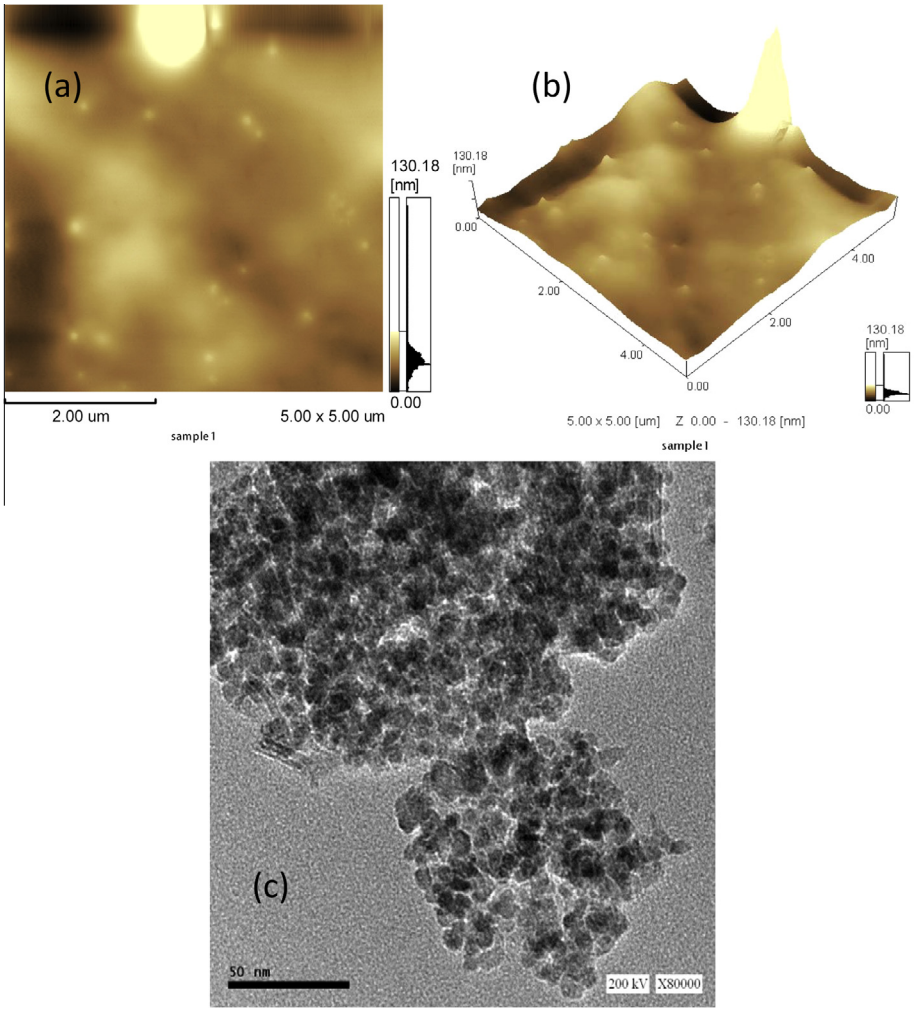

Fig. 4. Microphotographs of DETA-functionalized magnetic chitosan nano-based particles: (a) 2-D AFM, (b) 3-D AFM and (c) TEM photographs of the sorbent (the bar length is 50 nm).

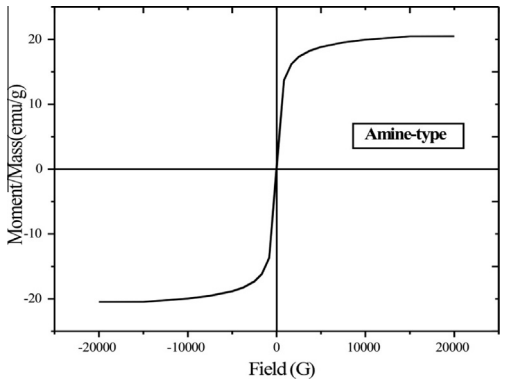

Fig. 5. Magnetization curves of DETA-functionalized magnetic chitosan nano-based particles.

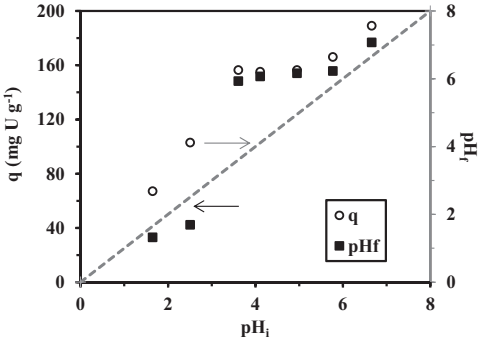

Fig. 6. Effect of initial pH on the sorption of U(VI) ions using DETA-functionalized magnetic chitosan nano-based particles: sorption capacity and equilibrium pH (C_0 = 110 mg U L^{-1}; T = 25 ± 1 °C; t = 1 h; sorbent dosage, SD = 0.2 g L^{-1}).

of pH on sorption performance: under similar conditions sorption capacity increases from 70 to 160 mg U g^{-1} when the pH increases from 1.65 to 4–6. The figure also shows strong variation of the pH during metal sorption (or due to the acid–base properties of the sorbent): while the pH slightly decreased in the range pH 1.6–2.4, it sharply increases above pH 2.5 to stabilize around pH 6. Above initial pH 6 (equilibrium pH above pH 7) the sorption capacity increases again, probably due to the formation of uranyl hydroxides, including polynuclear and polyhydrolyzed species: $UO_2(OH)^+$, $(UO_2)_2(OH)_2^{2+}$ or $(UO_2)_3(OH)_5^+$ and colloidal species that can precipitate in the solution or at the surface of the sorbent, under the form: $UO_2(OH)_2$ [49]. The pH stabilization around 6 can be correlated to the pK_a value of amine groups of chitosan, which is in the range 6.3–6.7 for conventional commercial chitosan

samples (the pK_a value depends on the degree of acetylation and the neutralization degree of amine functions) [50]. The adsorption efficiency increasing with the pH to reach a maximum at an equilibrium pH close to 6 can be also explained by the formation of an ion-pair between uranyl ions with sulfate anions (in sulfuric acid media), the neutralization of protonated amino groups that make them available for uranyl complexation (free electron doublet on nitrogen). The effect of pH on the sorption of uranyl ions has been documented on fungal biomass and chitosan derivative: optimum pH, dependent on metal concentration and pH, was correlated to the formation of polynuclear and polyhydrolyzed species [11,14]. For further experiments the pH was systematically fixed to 3.61 allowing maximum sorption capacity and preventing the pH variation to cause metal precipitation.

Ritcey and Ashbrook [51] reported the solvent extraction of uranyl ions from sulfuric acid solutions by amine-type extractants. The pH and the concentration of sulfate control metal speciation: the formation of anionic and neutral species being favorable. In acidic solutions, high concentrations of HSO_4^- are present and may react with uranyl ions to form uranium bisulfate poorly extractable. On the other hand, at high pH values (corresponding to sulfate excess), the amine functions, being unable to appear under their salt form, cannot extract anionic uranium sulfate species. The proper pH for uranyl extraction is expected to be in an intermediary range [51]. Based on this mechanism the sorption of uranyl ions in sulfuric acid media can be described by the following equations (Eqs. (5)–(9)) [52]:

$$UO_2^{2+} + 2SO_4^{2-} \rightarrow UO_2(SO_4)_2^{2-} \quad (5)$$

$$UO_2(SO_4)_2^{2-} + SO_4^{2-} \rightarrow UO_2(SO_4)_3^{4-} \quad (6)$$

The sorption mechanism of uranium using tertiary amines is essentially based on (a) the ability of metal ions to form anionic species in the aqueous phase, and (b) their capacity to be bound by amine groups through an anion-exchange process [52]. In a first step, the amine should be converted to the appropriate amine salt or polar ion-pair (Eq. (7a)). This makes possible, in a second step, the metal anions to be exchanged with the co-anion according to Eqs. (8a) and (9a):

$$2R_3N + H_2SO_4 \leftrightarrow (R_3NH^+)_2[SO_4]^{2-} \quad (7a)$$

$$2(R_3NH^+)_2[SO_4]^{2-} + UO_2(SO_4)_3^{4-} \leftrightarrow (R_3NH^+)_4[UO_2(SO_4)_3]^{4-} + 2SO_4^{2-} \quad (8a)$$

$$2(R_3NH^+)_2[SO_4]^{2-} + UO_2(SO_4)_2^{2-} \leftrightarrow (R_3NH^+)_2[UO_2(SO_4)_2]^{2-} + SO_4^{2-} \quad (9a)$$

By analogy with tertiary amines, similar reactions are expected with primary and secondary amines (hold by the chitosan derivative, see Fig. 1):

$$2R_2NH + H_2SO_4 \leftrightarrow (R_2NH_2^+)_2[SO_4]^{2-} \quad (7b)$$

$$2RNH_2 + H_2SO_4 \leftrightarrow (R_2NH_3^+)_2[SO_4]^{2-} \quad (7c)$$

$$2(R_2NH_2^+)_2[SO_4]^{2-} + UO_2(SO_4)_3^{4-} \leftrightarrow (R_2NH_2^+)_4[UO_2(SO_4)_3]^{4-} + 2SO_4^{2-} \quad (8b)$$

$$2(RNH_3^+)_2[SO_4]^{2-} + UO_2(SO_4)_3^{4-} \leftrightarrow (RNH_3^+)_4[UO_2(SO_4)_3]^{4-} + 2SO_4^{2-} \quad (8c)$$

$$2(R_2NH_2^+)_2[SO_4]^{2-} + UO_2(SO_4)_2^{2-} \leftrightarrow (R_2NH_2^+)_2[UO_2(SO_4)_2]^{2-} + SO_4^{2-} \quad (9a)$$

$$2(RNH_3^+)_2[SO_4]^{2-} + UO_2(SO_4)_2^{2-} \leftrightarrow (RNH_3^+)_2[UO_2(SO_4)_2]^{2-} + SO_4^{2-} \quad (9c)$$

For uranium from sulfate media, another extraction mechanism has been shown to operate for tertiary amines; namely the extraction of a neutral uranium sulfate species in an adduct-type mechanism [51]:

$$(R_3NH^+)_2[SO_4^{2-}] + UO_2SO_4 \leftrightarrow (R_3NH^+)_2[UO_2(SO_4)_2]^{2-} \quad (10a)$$

And by analogy:

$$(R_2NH_2^+)_2[SO_4^{2-}] + UO_2SO_4 \leftrightarrow (R_2NH_2^+)_2[UO_2(SO_4)_2]^{2-} \quad (10b)$$

$$(RNH_3^+)_2[SO_4^{2-}] + UO_2SO_4 \leftrightarrow (RNH_3^+)_2[UO_2(SO_4)_2]^{2-} \quad (10c)$$

Simsek et al. [53] investigate uranyl sorption on a resin grafted with DETA and propose the metal to be sorbed through chelation on amine groups (with contribution of carboxylic groups hold by the support). Sessler et al. [54] review the formation of uranium complexes with multidentate N-donor ligands: uranyl coordination may proceed through interactions with four, five or six N-donors. The affinity of the sorbent for uranyl ions is enhanced through the grafting of DETA since it increases the compactness, the volumetric density of chelating groups.

3.3.2. Uptake kinetics

Fig. 7 shows the uptake kinetics for uranyl ions using DETA-functionalized magnetic chitosan nano-based particles: the sorption capacity (q_t, mg U g^{-1}) is plotted *vs.* time (t). Two steps are identified: (a) the first stage that takes place for the first 40 min of contact and represents more than 99% of the total amount adsorbed, and (b) the second stage that lasts till 90 min of contact. Extended contact time (up to 180 min) have been carried out and they showed that increasing contact time (under selected experimental conditions) does not change residual concentration (Fig. AM1, see Additional Material Section). The initial stage corresponds to the fast sorption of uranyl ions due to (i) the strong affinity of the metal ions for DETA-functionalized chitosan (correlated to both the affinity of these reactive groups for uranyl ions and to the increased number of reactive amino groups), and (ii) the small size of magnetic chitosan nano-based particles (that limits the resistance to intraparticle diffusion and increases the surface of exchange of the sorbent with the solution) [18,29]. The second step in the process corresponds to a slow phenomenon limited by the strong decrease in the availability of sorption sites (most

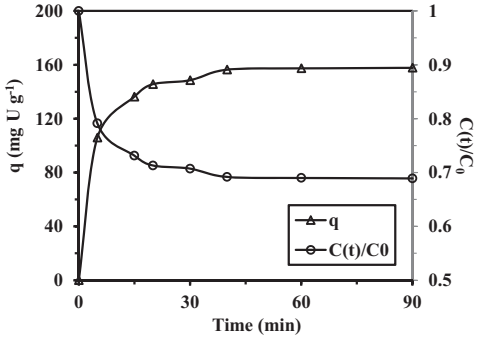

Fig. 7. Uptake kinetics for U(VI) sorption using DETA-functionalized magnetic chitosan nano-based particles (pH_i = 3.61 ; C_0 = 110 mg U L^{-1}; T = 25 ± 1 °C; SD = 0.2 g L^{-1}).

of them being occupied; this corresponds to the approach to saturation) while the hydrophilic behavior and the swelling properties of the biopolymer contribute to the additional sorption of small amounts of metal ions. Based on these results a contact time of about 40 min is sufficient to achieve the equilibrium: the residual sorption capacity is negligible for longer contact time (Fig. AM1, see Additional Material Section).

Uptake kinetics are generally controlled by a number of successive steps including (a) resistance to film diffusion, (b) resistance to intraparticle diffusion, and (c) the proper sorption reaction rate [55]. Providing a sufficient agitation allows reducing the impact of film diffusion (which usually plays a role within the first minutes of contact) and in most cases the uptake kinetics is controlled by the resistance to intraparticle diffusion and the sorption rate. Using nanoparticles contributes to reduce the impact of resistance to intraparticle diffusion. In order to verify these different hypotheses uptake kinetics have been modeled using various equations such as the pseudo-first order rate equation (PFORE), the pseudo-second order rate equation (PSORE) and the resistance to intraparticle diffusion (RIDE) [56]. The linear forms of pseudo-first-order and pseudo-second-order models are reported in Eqs. (11) and (12), respectively:

$$\log(q_e - q_t) = \log q_e - (k_1/2.303)t \tag{11}$$

$$t/q_t = 1/k_2 q_e^2 + (1/q_e)t \tag{12}$$

where q_e and q_t (mg g^{-1}) are the adsorption capacities at equilibrium and time t (min), respectively. k_1 (min^{-1}) and k_2 (g mg^{-1} min^{-1}) are the rate constant of pseudo-first order reaction and the rate constant of pseudo-second order reaction of sorption, respectively.

For systems controlled by the resistance to intraparticle diffusion complex models exist [55]; however, a first diagnostic on the impact of this mechanism on the control of uptake kinetics can be obtained using a simplified equation (Eq. (13)):

$$q_t = k_{int.} t^{0.5} + c \tag{13}$$

where q_t (mg g^{-1}) is the amount of metal ions adsorbed on the sorbent at time t (min), and $k_{\text{int.}}$ (mg g^{-1} min$^{-0.5}$) is the intraparticle diffusion constant.

The experimental data have been fitted by the aforementioned kinetics models; Table 1 reports the parameters of the models with their correlation coefficients. Table 1 clearly shows that the best fit of experimental data corresponds to the PSORE: the kinetics of sorption of uranyl ions on DETA-functionalized magnetic chitosan nano-based particles obeys a pseudo-second order rate equation. Fig. AM2 (See Additional Material Section) shows the linearized plot of experimental data according PSORE. Ones can assume that the rate limiting step in the sorption is the chemical sorption mechanism involving valence forces for sharing or exchanging electrons through complexation, coordination and chelation between sorbent surface and metal. Other models show poor correlation coefficient and this means that the relevant mechanisms

Table 1
Kinetics parameters for U(VI) ions sorption.

Pseudo-first order rate equation (PFORE)		
K_1 (min^{-1})	q_{eq} (mg U g^{-1})	R^2
9.76×10^{-2}	104.8	0.920
Pseudo-second order rate equation (PSORE)		
K_2 (g mg^{-1} min^{-1})	q_{eq} (mg U g^{-1})	R^2
3.66×10^{-3}	161. 3	0.999
Resistance to intraparticle diffusion equation (RIDE)		
c (mg U g^{-1})	K_p (mg U g^{-1} min$^{-0.5}$)	R^2
53.04	14.71	0.686

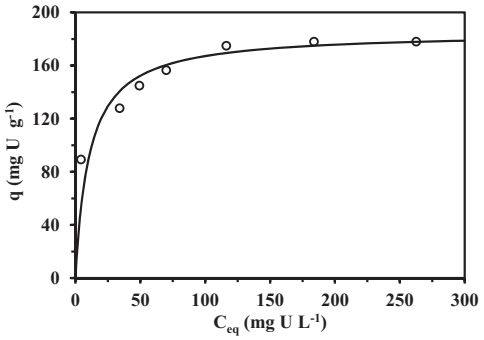

Fig. 8. Sorption isotherm for U(VI) using DETA-functionalized magnetic chitosan nano-based particles (pH$_i$ = 3.61; t = 40 min; T = 25 ± 1 °C; SD = 0.2 g L^{-1}).

are not playing a significant role in the control of uptake kinetics. As an example, Fig. AM3 (see Additional Material Section) shows the poor fit of experimental data for the simplified model of resistance to intraparticle diffusion.

3.3.3. Sorption isotherm and thermodynamic study

Fig. 8 shows the sorption isotherm for uranyl sorption using DETA-functionalized magnetic chitosan nano-based particles (initial pH: 3.6; T: 25 ± 1 °C). Sorption sharply increases with increasing residual concentration: sorption capacity reaches about 85 mg U g^{-1} for a residual uranium concentration close to 5 mg U L^{-1}. Then the sorption progressively increases to reach a plateau close to a residual concentration of 100 mg U L^{-1}: the maximum sorption capacity exceeds 160 mg U g^{-1}.

The adsorption equilibrium data have been analyzed using various isotherm models [57], such as the Langmuir, the Freundlich, and the Dubinin–Radushkevich (D–R) equations. The shape of the sorption isotherm with a saturation plateau is consistent with the mathematical equation representative of the Langmuir equation, contrary to the Freundlich equation that is characterized by a power-type equation (with exponential sorption capacity).

The Langmuir model is based on the assumption that: (a) adsorption sites are identical and energetically equivalent, (b) sorption occurs as a monolayer at the surface of the sorbent, [57,58]. The linearized form of the Langmuir equation is given by Eq. (14):

$$C_{eq}/q_e = (1/q_{m.})C_{eq} + (1/b \cdot q_{m.}) \tag{14}$$

where q_{max} is the sorption capacity at saturation of the monolayer of the sorbent (mg U g^{-1}), and b is the Langmuir adsorption constant (L mg^{-1}).

Experimental results are plotted using the linearized Langmuir equation (Fig. AM4, see Additional Material Section), and the

Table 2
Isotherm constants for U(VI) ions sorption.

Langmuir isotherm		
q_m	b (L mg^{-1})	R^2
185.2	0.093	0.998
Freundlich isotherm		
n	K_F (mg g^{-1})	R^2
5.53	69.7	0.967
Temkin isotherm		
A_T (L/mg)	B_T (Slope)	R^2
2.25	23.6	0.965
D–R isotherm		
$q_{max,D-R}$	E_{ad} (KJ mol^{-1})	R^2
174.3	8.39	0.931

parameters of the model are summarized in Table 2. The solid line on Fig. 8 shows the modeling of sorption isotherm using the parameters listed in Table 2. The simulated curve is close to experimental points as a confirmation of the suitability of the Langmuir equation to fit sorption isotherm.

To characterize the "favorability" of the sorption process a dimensionless constant (R_L) is usually calculated using the affinity coefficient of the Langmuir equation (b) [57]:

$$R_L = 1/(1 + b \cdot C_o) \quad (15)$$

All R_L values for the sorbent were from 0.035 to 0.326; all of them being smaller than 1, this means that uranyl sorption on DETA-functionalized magnetic chitosan nano-based particles is favorable, regardless of metal concentration.

Freundlich isotherm model is based on the assumption of an exponentially decaying adsorption site energy distribution [57,59]. It is applied to describe heterogeneous system and this is characterized by the heterogeneity factor, n. The linearized form of the Freundlich equation is given by Eq. (16):

$$\log q_e = \log k_f + 1/n \log C_e \quad (16)$$

where k_f is the Freundlich isotherm constant, and n (dimensionless) is the heterogeneity factor. Table 2 reports the value of the parameters: the value of the exponential term (i.e., $1/n$) being less than the unity the system can be considered as favorable; however, the correlation coefficient is much lower than in the case of the Langmuir equation.

Dubinin–Radushkevich (D–R) isotherm model is usually employed for the determination of the nature of the sorption process discriminating between physical and chemical mechanism. The linearized form of the D–R equation is given by [57,60]:

$$\ln q_e = \ln q_D - K_{DR}\varepsilon^2 \quad (17)$$

where q_D is the theoretical saturation capacity, and ε is the Polanyi potential, which is given by $\varepsilon = RT \ln(1 + 1/C_{eq})$. K_{DR} is correlated to the mean free adsorption energy per molecule of sorbate (according: $E_{DR} = (-2\ K)^{-1/2}$), R is the universal gas constant (8.314×10^{-3} kJ mol^{-1} K^{-1}) and T is the absolute temperature (K).

The D–R constant (K_{DR}) give valuable information on the mean energy of adsorption E_{DR} (kJ mol^{-1}). The plot of $\ln q_e$ *vs.* ε^2 gives a straight line with a slope K, and an intercept $\ln q_D$ as shown in Fig. AM5 (See Additional Material Section): the constants (such as q_D, and K_{DR}) are reported in Table 2. The mean adsorption energy (E_{DR}) corresponds to the free energy exchanged for the transfer of one mole of solute from infinity (in solution) to the surface of the sorbent. The calculated value of the mean adsorption energy (E_{DR}) is 8.4 kJ mol^{-1}: this is slightly higher than the value of 8 kJ mol^{-1}, which is usually selected for assigning the sorption process to a chemisorption mechanism. However, this is very close to the physisorption/chemisorption limit and a final conclusion will need complementary characterization, taking into account, for example, the effect of temperature (see below). Metal ions are strongly bonded to the reactive groups at the surface of the sorbent and this is consistent with the trends observed in the study of uptake kinetics (pseudo second order rate equation being the preferred model for sorption kinetics).

The Temkin isotherm was also tested for modeling sorption isotherm. The Temkin isotherm assumes that the free energy of biosorption is a function of the surface coverage [57,61]. The isotherm is described by Eq. (18):

$$q_e = B_T \ln C_{eq} + B_T \ln A_T \quad (18)$$

where A_T (L mg^{-1}) is the equilibrium binding constant corresponding to the maximum binding energy, B_T is a constant related to surface heterogeneity of the adsorbent, and T is the temperature (K). The constants of the Temkin model are reported in Table 2. A_T is correlated to the initial adsorption heat of sorption: the greater the A_T the higher the adsorption heat (and as a consequence, the greater the affinity of the sorbent for metal ions). Since the correlation coefficient is lower than for the Langmuir equation, the results should be taken as indicative values: the coefficient confirms the strong interaction between the metal and the reactive groups.

The thermodynamics of the sorption process was evaluated by comparing the sorption of uranyl ions by DETA-functionalized magnetic chitosan nanoparticles under similar conditions (same initial concentration; i.e., C_0: 209 mg U L^{-1}; SD: 0.2 g L^{-1}) at different temperatures (in the range 298–323 K) (See Table 3). The sorption of uranyl ions decreases from 175 mg U g^{-1} to 123 mg U g^{-1} with increasing the temperature from 298 to 323 K: the reaction is exothermic. This is confirmed by the determination of the enthalpy change of the reaction ($\Delta H°$) using the Van't Hoff equation (logarithmic plot of the distribution coefficient *vs.* the reciprocal of the temperature) [52] (Fig. 9):

$$\ln K_d = (-\Delta H°/R)/T + \Delta S°/R \quad (19)$$

The values of $\Delta H°$ (−12.45 kJ mol^{-1}) and $\Delta S°$ (the entropy change, 62 J mol^{-1} K^{-1}) are reported in Table 3, together with the Gibbs free energy, $\Delta G°$ (calculated using Eq. (20)). The negative value of $\Delta H°$ confirms the exothermic nature of the sorption process. The exothermic nature of adsorption has also been reported for U(VI) adsorption on ethylenediamine-modified magnetic chitosan [29], magnetic Schiff base [43], and ion-imprinted and non-imprinted magnetic chitosan-based resins [62]. On the other hand the sorption of U(VI) has been reported to be endothermic using tetraethylenepentamine/glycidyl methacrylate chelating resin [9], salicylideneimine–functionalized hydrothermal carbon [5], and Amberlite IRA-910 resin [52].

$$\Delta G° = \Delta H° - T\Delta S° \quad (20)$$

The negative values of $\Delta G°$ indicate the spontaneous nature of the sorption process: their decrease with increasing the temperature confirms that the sorption is more efficient at low

Table 3
Thermodynamic parameters of U(VI) ions sorption.

Temp. (K)	$\Delta H°$ (KJ mol^{-1})	$\Delta S°$ (J mol^{-1})	ΔG, (KJ mol^{-1})	$T\Delta S°$ (KJ mol^{-1})	R^2
298	−12.450	62	−30.78	18.33	0.981
308			−31.39	18.94	
313			−31.70	19.25	
318			−32.32	19.56	
323			−32.30	19.87	

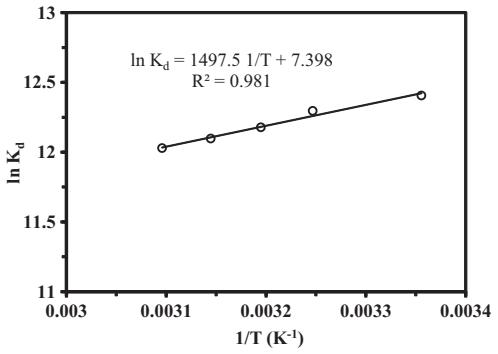

Fig. 9. Van't Hoff plots of $\ln K_d$ against $1/T$, (K^{-1}) for U(VI) sorption using DETA-functionalized magnetic chitosan nano-based particles (pH$_i$ = 3.61; t = 40 min; C_0: 200 mg U L^{-1}; SD = 0.2 g L^{-1}).

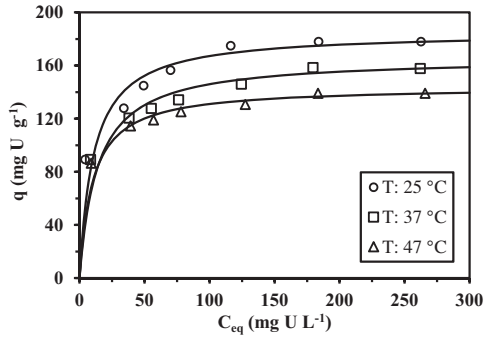

Fig. 10. Sorption isotherm for U(VI) using DETA-functionalized magnetic chitosan nano-based particles at different temperatures (pH_i = 3.61; t = 40 min; SD = 0.2 g L^{-1}).

temperature [5]. In addition, the fact that $|\Delta H°| < |T\Delta S°|$ in the whole range of studied temperatures means that the adsorption process was dominated by entropy rather than enthalpy changes [52]. The positive value of the entropy change means that the randomness increases of the solid/liquid interface, possibly due to dissociation of complexes, release of exchangeable ions etc. These trends are confirmed by the comparison of sorption isotherms obtained at T: 25, 37 and 47 °C (Fig. 10). The maximum sorption capacity at saturation of the monolayer (q_m in the Langmuir equation) decreases from 185 mg U g^{-1} at 25 °C to 166 and 144 mg U g^{-1} when increasing temperature to 37 °C and 47 °C, respectively. On the other hand, the coefficient b of the Langmuir equation varies between 0.073 L mg^{-1} (at 37 °C) and 0.1 L mg^{-1} (at 47 °C and 0.093 L mg^{-1} at 25 °C). Increasing the temperature decreases uranyl sorption performance: the reaction is exothermic. The negative effect of temperature is usually associated to a physisorption mechanism. This is globally consistent with the value of the E_{DR} found above, which is close to the "frontier" between physisorption and chemisorption. Contradictory conclusions have been reported by different research groups using similar sorbents. Elwakeel et al. [23] report the negative impact of temperature on uranium sorption using tetraethylenepentamine-modified magnetic chitosan resins and the E_{DR} was less than 2 kJ mol^{-1}. On the other hand, Xu et al. [22] obtained E_{DR} slightly higher than 9 kJ mol^{-1} for U(VI) sorption on diethyleneamine-functionalized magnetic chitosan: they conclude on the predominance of chemisorption mechanism.

Table 4
Comparison of adsorption capacity for UO_2^{2+} ions for various sorbents.

Adsorbents	Equilibration time (min)	Adsorption capacity (mg U g^{-1})	References
Magnetite nanoparticles	300	5	[63]
Magnetic chitosan	40	42	[64]
Cross-linked chitosan with epichlorohydrin	180	49.05	[44]
Ethylenediamine-modified magnetic chitosan	30	82.83	[29]
Tetraethylenepentamine/ glycidyl methacrylate	60	460.3	[9]
Salicylideneimine/ functionalized hydrothermal carbon	120	261.8	[5]
Magnetic Schiff base	360	94.3	[43]
Amberlite IRA-910 resin	120	11.90	[52]
Ion-imprinted magnetic chitosan resins	180	187.26	[62]
Non-imprinted magnetic chitosan resins	180	160.77	[62]
Amine-functionalized magnetic-chitosan nano-based particles	40	177.93	This work

Table 5
Sorption/desorption cycles: sorption capacity and sorption efficiency.

Cycle	q_e (mg g^{-1})	Ads. (%)
Cycle I	177.7	100
Cycle II	166.0	93.4
Cycle III	157.3	88.5
Cycle IV	157.2	88.5
Cycle V	157.5	88.6
Cycle VI	154.9	87.2

Table 4 compares the maximum sorption capacities of various sorbents for UO_2^{2+} ions. Since these experiments were not systematically obtained under similar experimental conditions, the strict comparison of absolute values is not easy; this simply gives an overview of the potential of the present sorbent against other materials. Although these data were obtained under different experimental conditions, they represent a useful criterion for comparison of adsorption capacities. Table 4 confirms that DETA-functionalized magnetic chitosan nano-based particles have very competitive sorption performance in terms of both sorption capacity and uptake kinetics. Table AM1 (See Additional Material Section) complete these data with additional information on uranyl sorption performance of the DETA-functionalized chitosan nano-based particles with comparison to other sorbents (based on chitosan, modified chitosan, synthetic resins).

3.4. Regeneration studies

The desorption of metal ions from loaded sorbents is generally performed using acidic solutions such as HCl or HNO_3. In the present case, acidic conditions may cause the denaturation (dissolving and destruction) of the magnetic core of sorbent particles. It was necessary testing alternative eluants such as ethylenediamine tetraacetic acid (EDTA), thiourea and urea, which are known for being strong chelating agents for many metal ions. Preliminary tests showed that a solution of urea (0.5 M) acidified with a few drops of H_2SO_4 (0.2 M) efficiently desorbed uranyl ions: 30 min of contact were sufficient for achieving the desorption equilibrium. The sorption and desorption steps were repeated five times. Table 5 reports the evolution of sorption capacity and sorption efficiency at the different cycles. A progressive decrease of the sorption capacity (and sorption efficiency is observed). However, the sorption capacity decreased by less than 7% at the second step and by less than 12% at the third step, while the decrease in sorption capacity tended to stabilize after this third cycle (decrease by less than 13% at the sixth cycle). The mechanism of desorption (and sorbent regeneration) is associated to electrostatic and complexation/chelation reactions.

The grafting of supplementary and highly reactive amine groups, the synthesis of nanoparticles with large surface area may explain the good sorption performance of the synthesized material. The possibility to recover the sorbent by external magnetic field contributes to make these materials very interesting for applications in hazardous conditions.

4. Conclusion

Diethylenetriamine functionalized magnetic chitosan nano-based particles have been synthesized, characterized and efficiently tested for U(VI) recovery from synthetic sulfuric acid media.

The maximum sorption capacity was found close to 178 mg g^{-1} for uranium ions at pH 3.61 (initial pH that raises up to 5.5–6), initial concentration 200 mg U L^{-1} and temperature 25 ± 1 °C. Temperature shows a negative effect on UO_2^{2+} ions adsorption: the reaction is exothermic (ΔH° = −12.45 kJ mol^{-1}), spontaneous (ΔG° around −32 kJ mol^{-1}) and increased randomness after metal sorption (ΔS° = +62 J mol^{-1} K^{-1}). Uptake kinetics are modeled with the pseudo-second order rate equation: the contribution of resistance to intraparticle diffusion is limited by the nanometric size of sorbent particles that offer large surface areas for interaction with metal ions. The Langmuir equation fits well sorption isotherm compared to other conventional models. Finally, the adsorbent can be efficiently regenerated by acidified urea (0.5 mol L^{-1}) as the eluent: the loss in sorption capacity and efficiency does not exceed 13% at the sixth sorption/desorption cycle.

Acknowledgments

This work was supported by the French Government through a fellowship granted by the French Embassy in Egypt (Institut Français d'Egypte). Special dedication to the memory of Prof. Dr. Ahmed Donia.

Appendix A. Supplementary data

Supplementary data associated with this article can be found, in the online version, at http://dx.doi.org/10.1016/j.cej.2014.09.061.

References

[1] M.W. Clark, J.J. Harrison, T.E. Payne, The pH-dependence and reversibility of uranium and thorium binding on a modified bauxite refinery residue using isotopic exchange techniques, J. Colloid Interface Sci. 356 (2011) 699–705.
[2] Y. Arai, C.C. Fuller, Effects of sulfate ligand on uranyl carbonato surface species on ferrihydrite surfaces, J. Colloid Interface Sci. 365 (2012) 268–274.
[3] X.P. Liao, Z.B. Lu, X. Du, X. Liu, B. Shi, Collagen fiber immobilized *Myrica rubra* tannin and its adsorption to UO_2^{2+}, Environ. Sci. Technol. 38 (2004) 324–328.
[4] M.G. Roig, T. Manzano, M. Diaz, Biochemical process for the removal of uranium from acid mine drainages, Water Res. 31 (1997) 2073–2083.
[5] H. Wang, L. Ma, K. Cao, J. Geng, J. Liu, Q. Song, X. Yang, S. Li, Selective solid-phase extraction of uranium by salicylideneimine-functionalized hydrothermal carbon, J. Hazard. Mater. 229 (2012) 321–330.
[6] P. Michard, E. Guibal, T. Vincent, P. LeCloirec, Sorption and desorption of uranyl ions by silica gel: pH, particle size and porosity effects, Micropor. Mater. 5 (1996) 309–324.
[7] M. Zavarin, S.K. Roberts, N. Hakem, A.M. Sawvel, A.B. Kersting, Eu(III), Sm(III), Np(V), Pu(V), and Pu(IV) sorption to calcite, Radiochim. Acta 93 (2005) 93–102.
[8] J. Roosen, K. Binnemans, Adsorption and chromatographic separation of rare earths with EDTA- and DTPA-functionalized chitosan biopolymers, J. Mater. Chem. A 2 (2014) 1530–1540.
[9] A.M. Donia, A.A. Atia, E.M.M. Moussa, A.M. El-Sherif, M.O.A. El-Magied, Removal of uranium(VI) from aqueous solutions using glycidyl methacrylate chelating resins, Hydrometallurgy 95 (2009) 183–189.
[10] A.M. Donia, A.A. Atia, A.M. Daher, O.A. Desouky, E.A. Elshehy, Synthesis of amine/thiol magnetic resin and study of its interaction with Zr(IV) and Hf(IV) ions in their aqueous solutions, J. Dispersion Sci. Technol. 32 (2011) 634–641.
[11] E. Guibal, C. Roulph, P. Le Cloirec, Uranium biosorption by a filamentous fungus *Mucor miehei*: pH effect on mechanisms and performances of uptake, Water Res. 26 (1992) 1139–1145.
[12] G. Haferburg, D. Merten, G. Büchel, E. Kothe, Biosorption of metal and salt tolerant microbial isolates from a former uranium mining area. Their impact on changes in rare earth element patterns in acid mine drainage, J. Basic Microbiol. 47 (2007) 474–484.
[13] G. Naja, C. Mustin, B. Volesky, J. Berthelin, Biosorption study in a mining wastewater reservoir, Int. J. Environ. Pollut. 34 (2008) 14–27.
[14] E. Guibal, I. Saucedo, J. Roussy, P. Lecloirec, Uptake of uranyl ions by new sorbing polymers – discussion of adsorption-isotherms and pH effect, React. Polym. 23 (1994) 147–156.
[15] M. Jansson Charrier, E. Guibal, J. Roussy, R. Surjous, P. LeCloirec, Dynamic removal of uranium by chitosan: influence of operating parameters, Water Sci. Technol. 34 (1996) 169–177.
[16] E. Guibal, Interactions of metal ions with chitosan-based sorbents: a review, Sep. Purif. Technol. 38 (2004) 43–74.
[17] I. Saucedo, E. Guibal, J. Roussy, C. Roulph, P. Lecloirec, Uranium sorption by glutamate glucan – a modified chitosan. 1. Equilibrium studies, Water SA 19 (1993) 113–118.
[18] S.K. Shukla, A.K. Mishra, O.A. Arotiba, B.B. Mamba, Chitosan-based nanomaterials: a state-of-the-art review, Int. J. Biol. Macromol. 59 (2013) 46–58.
[19] R. Jayakumar, M. Prabaharan, R.L. Reis, J.F. Mano, Graft copolymerized chitosan – present status and applications, Carbohydr. Polym. 62 (2005) 142–158.
[20] G. Wang, J. Liu, X. Wang, Z. Xie, N. Deng, Adsorption of uranium (VI) from aqueous solution onto cross-linked chitosan, J. Hazard. Mater. 168 (2009) 1053–1058.
[21] A.A. Atia, Studies on the interaction of mercury(II) and uranyl(II) with modified chitosan resins, Hydrometallurgy 80 (2005) 13–22.
[22] J. Xu, M. Chen, C. Zhang, Z. Yi, Adsorption of uranium(VI) from aqueous solution by diethylenetriamine-functionalized magnetic chitosan, J. Radioanal. Nucl. Chem. 298 (2013) 1375–1383.
[23] K.Z. Elwakeel, A.A. Atia, E. Guibal, Fast removal of uranium from aqueous solutions using tetraethylenepentamine modified magnetic chitosan resin, Bioresour. Technol. 160 (2014) 107–114.
[24] I.W. Mwangi, J.C. Ngila, Removal of heavy metals from contaminated water using ethylenediamine-modified green seaweed (*Caulerpa serrulata*), Phys. Chem. Earth 50–52 (2012) 111–120.
[25] M.E.H. Ahamed, X.Y. Mbianda, A.F. Mulaba-Bafubiandi, L. Marjanovic, Selective extraction of gold(III) from metal chloride mixtures using ethylenediamine N-(2-(1-imidazolyl)ethyl) chitosan ion-imprinted polymer, Hydrometallurgy 140 (2013) 1–13.
[26] P.D. Chethan, B. Vishalakshi, Synthesis of ethylenediamine modified chitosan and evaluation for removal of divalent metal ions, Carbohydr. Polym. 97 (2013) 530–536.
[27] F.-N. Allouche, E. Guibal, N. Mameri, Preparation of a new chitosan-based material and its application for mercury sorption, Colloids Surf. A 446 (2014) 224–232.
[28] X. Xue, J. Wang, L. Mei, Z. Wang, K. Qi, B. Yang, Recognition and enrichment specificity of Fe_3O_4 magnetic nanoparticles surface modified by chitosan and *Staphylococcus aureus* enterotoxins A antiserum, Colloids Surf. B 103 (2013) 107–113.
[29] J.-S. Wang, R.-T. Peng, J.-H. Yang, Y.-C. Liu, X.-J. Hu, Preparation of ethylenediamine-modified magnetic chitosan complex for adsorption of uranyl ions, Carbohydr. Polym. 84 (2011) 1169–1175.
[30] G. Dodi, D. Hritcu, G. Lisa, M.I. Popa, Core-shell magnetic chitosan particles functionalized by grafting: synthesis and characterization, Chem. Eng. J. 203 (2012) 130–141.
[31] Z. Marczenko, Spectrophotometric Determination of Elements, Ellis Horwood, Chichester (U.K.), 1976.
[32] M. Namdeo, S.K. Bajpai, Chitosan-magnetite nanocomposites (CMNs) as magnetic carrier particles for removal of Fe(III) from aqueous solutions, Colloids Surf. A 320 (2008) 161–168.
[33] W.S. Wan Ngah, C.S. Endud, R. Mayanar, Removal of copper(II) ions from aqueous solution onto chitosan and cross-linked chitosan beads, React. Funct. Polym. 50 (2002) 181–190.
[34] K. Oshita, T. Takayanagi, M. Oshima, S. Motomizu, Adsorption behavior of cationic and anionic species on chitosan resins possessing amino acid moieties, Anal. Sci. 23 (2007) 1431–1434.
[35] K.Z. Elwakeel, A.A. Atia, A.M. Donia, Removal of Mo(VI) as oxoanions from aqueous solutions using chemically modified magnetic chitosan resins, Hydrometallurgy 97 (2009) 21–28.
[36] L. Martinez, F. Agnely, B. Leclerc, J. Siepmann, M. Cotte, S. Geiger, G. Couarraze, Cross-linking of chitosan and chitosan/poly(ethylene oxide) beads: a theoretical treatment, Eur. J. Pharm. Biopharm. 67 (2007) 339–348.
[37] M.S. Dzul Erosa, T.I. Saucedo Medina, R. Navarro Mendoza, M. Avila Rodriguez, E. Guibal, Cadmium sorption on chitosan sorbents: kinetic and equilibrium studies, Hydrometallurgy 61 (2001) 157–167.
[38] M. Ruiz, A.M. Sastre, E. Guibal, Palladium sorption on glutaraldehyde-crosslinked chitosan, React. Funct. Polym. 45 (2000) 155–173.
[39] V.L. Gonçalves, M.C.M. Laranjeira, V.T. Fávere, R.C. Pedrosa, Effect of crosslinking agents on chitosan microspheres in controlled release of diclofenac sodium, Polim. Cienc. Tecnol. 15 (2005) 6–12.
[40] E.M. Soliman, M.E. Mahmoud, S.A. Ahmed, Synthesis, characterization and structure effects on selectivity properties of silica gel covalently bonded diethylenetriamine mono- and bis-salicylaldehyde and naphthaldehyde Schiff's bases towards some heavy metal ions, Talanta 54 (2001) 243–253.
[41] G.R. Kiani, H. Sheikhloie, N. Arsalani, Heavy metal ion removal from aqueous solutions by functionalized polyacrylonitrile, Desalination 269 (2011) 266–270.
[42] A. Khan, S. Badshah, C. Airoldi, Biosorption of some toxic metal ions by chitosan modified with glycidylmethacrylate and diethylenetriamine, Chem. Eng. J. 171 (2011) 159–166.
[43] X. Zhang, C. Jiao, J. Wang, Q. Liu, R. Li, P. Yang, M. Zhang, Removal of uranium(VI) from aqueous solutions by magnetic Schiff base: kinetic and thermodynamic investigation, Chem. Eng. J. 198 (2012) 412–419.
[44] M. Hosoba, K. Oshita, R.K. Katarina, T. Takayanagi, M. Oshima, S. Motomizu, Synthesis of novel chitosan resin possessing histidine moiety and its application to the determination of trace silver by ICP-AES coupled with triplet automated-pretreatment system, Anal. Chim. Acta 639 (2009) 51–56.

[45] A. Guinier, P. Lorrain, D. Sainte-Marie Lorrain, X-ray diffraction, in: E. Daniel (Ed.), Crystals, Imperfect Crystals and Amorphous Bodies, W.H. Freeman & Co, San Francisco, CA, 1963.
[46] Z. Zhou, F. Jiang, T.-C. Lee, T. Yue, Two-step preparation of nano-scaled magnetic chitosan particles using Triton X-100 reversed-phase water-in-oil microemulsion system, J. Alloys Compd. 581 (2013) 843–848.
[47] A. Hasanpour, M. Niyaifar, H. Mohammadpour, J. Amighian, A novel non-thermal process of TiO_2-shell coating on Fe_3O_4-core nanoparticles, J. Phys. Chem. Solids 73 (2012) 1066–1070.
[48] G. Crini, H.N. Peindy, F. Gimbert, C. Robert, Removal of CI basic green 4 (Malachite Green) from aqueous solutions by adsorption using cyclodextrin-based adsorbent: kinetic and equilibrium studies, Sep. Purif. Technol. 53 (2007) 97–110.
[49] C.F. Baes Jr., R.E. Mesmer, Hydrolysis of Cations, Wiley, NY, 1976.
[50] P. Sorlier, A. Denuzière, C. Viton, A. Domard, Relation between the degree of acetylation and the electrostatic properties of chitin and chitosan, Biomacromolecules 2 (2001) 765–772.
[51] G.M. Ritcey, A.W. Ashbrook, Solvent Extraction: Principles and Applications to Process Metallurgy, Elsevier, Amsterdam, NL, 1984.
[52] A. Rahmati, A. Ghaemi, M. Samadfam, Kinetic and thermodynamic studies of uranium(VI) adsorption using Amberlite IRA-910 resin, Ann. Nucl. Energy 39 (2012) 42–48.
[53] S. Simsek, E. Yilmaz, A. Boztug, Amine-modified maleic anhydride containing terpolymers for the adsorption of uranyl ion in aqueous solutions, J. Radioanal. Nucl. Chem. 298 (2013) 923–930.
[54] J.L. Sessler, P.J. Melfi, G.D. Pantos, Uranium complexes of multidentate N-donor ligands, Coord. Chem. Rev. 250 (2006) 816–843.
[55] C. Tien, Adsorption Calculations and Modeling, Butterworth-Heinemann, Newton, MA, 1994.
[56] H. Qiu, L. Lv, B. Pan, Q. Zhang, W. Zhang, Q. Zhang, Review: critical review in adsorption kinetic models, J. Zhejiang Univ. Sci. A 10 (2009) 716–724.
[57] K.Y. Foo, B.H. Hameed, Insights into the modeling of adsorption isotherm systems, Chem. Eng. J. 156 (2010) 2–10.
[58] I. Langmuir, The adsorption of gases on plane surfaces of glass, mica and platinum, J. Am. Chem. Soc. 40 (1918) 1361–1402.
[59] H.M.F. Freundlich, Uber die adsorption in lasungen, Z. Phys. Chem. 57 (1906) 385–470.
[60] M.M. Dubinin, E.D. Zaverina, L.V. Radushkevich, Sorption and structure of active carbons. I. Adsorption of organic vapors, Zh. Fiz. Khim. 21 (1947) 1351–1362.
[61] V.P. Temkin, Kinetics of ammonia synthesis on promoted iron catalysts, Acta Physiochim. 12 (1940) 217–222.
[62] L. Zhou, C. Shang, Z. Liu, G. Huang, A.A. Adesina, Selective adsorption of uranium(VI) from aqueous solutions using the ion-imprinted magnetic chitosan resins, J. Colloid Interface Sci. 366 (2012) 165–172.
[63] D. Das, M.K. Sureshkumar, S. Koley, N. Mithal, C.G.S. Pillai, Sorption of uranium on magnetite nanoparticles, J. Radioanal. Nucl. Chem. 285 (2010) 447–454.
[64] L.C.B. Stopa, M. Yamaura, Uranium removal by chitosan impregnated with magnetite nanoparticles: adsorption and desorption, Int. J. Nucl. Energy Sci. Technol. 5 (2010) 283–289.